THE JOURNAL OF BIOLOGICAL CHEMISTRY
Vol. 280, No. 19, Issue of May 13, pp. 18833–18841, 2005
Printed in U.S.A.

Structure of the Intermolecular Complex between Plastocyanin and Cytochrome *f* from Spinach*[S]

Received for publication, November 11, 2004, and in revised form, January 24, 2005
Published, JBC Papers in Press, February 3, 2005, DOI 10.1074/jbc.M412760200

Francesco Musiani‡§, Alexander Dikiy‡§¶, Alexey Yu Semenov‖, and Stefano Ciurli‡***

From the ‡Laboratory of Bioinorganic Chemistry, Department of Agro-Environmental Science and Technology, University of Bologna, Viale Giuseppe Fanin 40, 40127 Bologna, Italy and ‖A. N. Belozersky Institute of Physico-Chemical Biology, Moscow State University, 119899 Moscow, Russia

In oxygenic photosynthesis, plastocyanin shuttles electrons between the membrane-bound complexes cytochrome b_6f and photosystem I. The homologous complex between cytochrome *f* and plastocyanin, both from spinach, is the object of this study. The solution structure of the reduced spinach plastocyanin was determined using high field NMR spectroscopy, whereas the model structure of oxidized cytochrome *f* was obtained by homology modeling calculations and molecular dynamics. The model structure of the intermolecular complex was calculated using the program AUTODOCK, taking into account biological information obtained from mutagenesis experiments. The best electron transfer pathway from the heme group of cytochrome *f* to the copper ion of plastocyanin was calculated using the program HARLEM, obtaining a coupling decay value of 1.8×10^{-4}. Possible mechanisms of interaction and electron transfer between plastocyanin and cytochrome *f* were discussed considering the possible formation of a supercomplex that associates one cytochrome b_6f, one photosystem I, and one plastocyanin.

Plastocyanin (Pc)[1] and cytochrome (Cyt) *f* are redox proteins in the electron transfer chain of eukaryotic and prokaryotic oxygenic photosynthesis. Cyt *f*, an integral part of plastoquinol:plastocyanin oxidoreductase (Cyt b_6f complex, EC 1.10.99.1) (1, 2), accepts electrons from the Rieske FeS protein in the Cyt b_6f complex. Electrons are subsequently transferred onto the soluble luminal electron carrier Pc, which in turn reduces $P700^+$, the photooxidized primary electron donor in photosystem I (PS I) (3). The functional role and mechanism of the Cyt b_6f complex is analogous to that of ubiquinol:cytochrome *c* oxidoreductase (Cyt bc_1 complex) in mitochondria and bacteria (4). This functional analogy derives from the large similarity between the molecular structure of Cyt bc_1 (5–8) and that of Cyt b_6f (9, 10).

In the structure of the Cyt b_6f complex, the Cyt *f* subunit is anchored in the thylakoid membrane through a single membrane-spanning α-helix near the C terminus. The redox-active 28-kDa N-terminal domain of this subunit (Cyt *f*) protrudes into the lumen and can be isolated in a soluble form detached from the membrane-anchoring helix (11). The crystal structures of the soluble Cyt *f* domain from *Brassica campestris* (turnip) (12), thermophilic cyanobacterium *Phormidium laminosum* (13), and green alga *Chlamydomonas reinhardtii* (14) have been determined and revealed that the overall fold of the domain is largely coincident with the same domain in the full Cyt b_6f complex. Cyt *f* is an elongated molecule composed of two domains (Fig. 1*A*, *left panel*). The larger domain has an immunoglobulin-like fold composed by a three-layer structure made of β-strands flanked by small α-helices. The small domain is also composed of β-strands folded into a small "jelly roll." The heme group nestles between two short helices near the N terminus of Cyt *f* and is covalently bound to the protein by thioether bonds through strictly conserved cysteine residues in the fingerprint peptide Cys-*X*-*Y*-Cys-His sequence found in all of the *c*-type cytochromes. The heme Fe(III)/(II) is axially bound by a proximal His^{25} Nε and by the α-amino group of the N-terminal residue Tyr^1 (Fig. 1*A*, *right panel*).

The Cyt *f* redox partner plastocyanins are small (~10 kDa) soluble proteins belonging to a larger class of metalloproteins, named blue copper proteins, containing copper in their active site (15). Several structures of plastocyanins from different biological sources, derived using both solid-state x-ray crystallography and solution NMR spectroscopy, indicate that these proteins consist of a highly conserved antiparallel β-barrel structure (Fig. 1*B*, *top panel*). The Cu(II)/(I) ion is found in a so-called type I center bound to one Cys Sγ and two His Nδ residues in a distorted trigonal planar structure with a weakly bound axial Met Sδ (Fig. 1*B*, *bottom panel*).

The complex formed between spinach Pc and turnip Cyt *f* is characterized by a high dissociation rate (16), suggesting that the interaction is short-lived, thus preventing a structural study using x-ray crystallography. Several different computational approaches to elucidate the structure of the bimolecular complex formed between spinach or poplar Pc and turnip Cyt *f* have been employed. Manual docking was first attempted us-

* This work was supported by INTAS Grant 01-483 (to S. C. and A. Y. S.), by the International Science and Technology Center Grant 2296 (to A. Y. S.), by Grants PRIN-2001 and PRIN-2003 from the Ministero Italiano dell'Università e della Ricerca (to S. C.), and by the Russian Foundation for Basic Research (Grant 03-04-48983) (to A. Y. S.). The costs of publication of this article were defrayed in part by the payment of page charges. This article must therefore be hereby marked "*advertisement*" in accordance with 18 U.S.C. Section 1734 solely to indicate this fact.

[S] The on-line version of this article (available at http://www.jbc.org) contains Supplemental Table I and Fig. 1.

The atomic coordinates and structure factors (code 1YLB) have been deposited in the Protein Data Bank, Research Collaboratory for Structural Bioinformatics, Rutgers University, New Brunswick, NJ (http://www.rcsb.org/).

§ Recipient of fellowships provided by Consorzio Interuniversitario per le Risonanze Magnetiche di Metalloproteine Paramagnetiche (CIRMMP).

¶ Present address: Dept. of Biotechnology, Norwegian University of Science and Technology, Trondheim, NO-7491, Norway.

** To whom correspondence should be addressed: Dept. of Agro-Environmental Science and Technology, Laboratory of Bioinorganic Chemistry, University of Bologna, Viale Giuseppe Fanin 40, 40127 Bologna, Italy. Tel.: 39-051-209-6204; Fax: 39-051-209-6203; E-mail: stefano.ciurli@unibo.it.

[1] The abbreviations used are: Pc, plastocyanin; Cyt, cytochrome; Cyt *f*, soluble domain of cytochrome *f*; NMR, nuclear magnetic resonance; PS I, photosystem I; P700, primary electron donor in photosystem I; r.m.s.d., root mean square deviation.

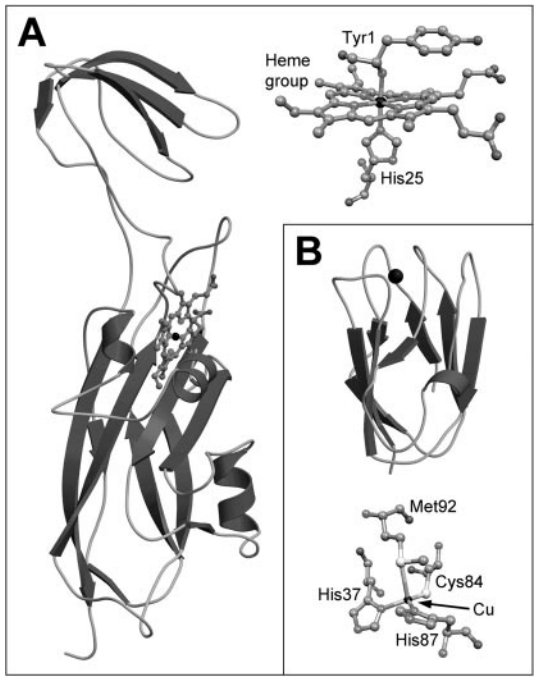

FIG. 1. *A*, ribbon diagram of turnip Cyt *f* (*left panel*) revealing the position of the heme group shown in *ball-and-stick* representation in the *right panel*. *B*, ribbon diagram of mutant spinach Pc (*top panel*) revealing the position of the type I copper center shown in *ball-and-stick* representation in the *bottom panel*. The metal ions are shown as *black spheres* of arbitrary radius.

ing information derived by mapping the electrostatic field on the proteins surface (17, 18). Subsequently, molecular dynamics (19) and Brownian dynamics (20, 21) were employed. The structures calculated using these pure computational methods suggest the existence of several different orientations used by the two proteins to approach each other. The use of experimental constraints derived from NMR in combination with restrained rigid body molecular mechanics yielded a family of highly similar structures of the transient complex between spinach Pc and turnip Cyt *f* (22–24). These structures reveal that van der Waals interactions between the heme region of Cyt *f* and the hydrophobic patch of Pc bring the two metal ions, iron and copper, within ~11 Å of each other. Additionally, the interaction within this complex is proposed between basic and acidic patches on Cyt *f* and Pc surface, respectively. This conclusion is supported by site-directed mutagenesis studies on residues within either of these two electrostatically complementary regions, resulting in a decrease of the electron transfer rate (16, 25–27).

Although the overall molecular structure is very similar for various plastocyanins, the surface properties are not conserved among all of the members of this class of proteins with the surface electrostatic potential features differing between plant and prokaryotic members of this family. Higher plant plastocyanins are characterized by rather similar surface features confirmed by the conserved net charge at pH 7 (-9 ± 1) (28), whereas cyanobacterial plastocyanins have a widely varying net charges. As a result, one of the functionally relevant plant plastocyanins patches, the so-called acidic or eastern patch, is barely observed in the case of the bacterial proteins. These differences in surface charge properties have a profound influence on the kinetics of the interaction between Cyt *f* and Pc (29, 30).

The structures of the transient homologous complexes formed by Cyt *f* and Pc from the cyanobacteria *Phormidium laminosum* (31) and *Prochlorothrix hollandica* (32) were determined by the same combination of NMR and computational methodology used in the case of the heterologous complexes of higher plants proteins. The complexes are less well defined with respect to the higher plant counterpart because of either the increased mobility within the cyanobacterial complex or the lower number of restraints used in calculations. In the case of these cyanobacterial protein complexes, none of the lowest energy structures was similar to the higher plant analogues, possibly because of different surface characteristics of bacterial and plants redox partners. This suggestion is confirmed by the absence of electrostatic charges involved in the cyanobacterial complex, which instead appears to entail mainly hydrophobic interactions. However, the role of electrostatic interactions in the *P. laminosum* Pc-Cyt *f* complex involving the same basic/acidic patches observed in the heterologous complex formed in the case of higher plants has been established by kinetic measurements on site-directed Pc and Cyt *f* mutants (31, 32). These results suggest that the charged patches are important for the formation of the encounter complex, which involves transient conformations that are invisible by NMR. These electrostatic interactions were suggested to increase the number of productive collisions to form the reaction complex in a diffusion-limited mechanism.

The missing piece of this puzzle is represented by the lack of information on the structure of a homologous complex between Pc and Cyt *f* from higher plants. One of the reasons why it is important to study homologous complexes is the possibility of establishing well defined shape and charge complementarity between interacting proteins. In this work, we present a modeled structure of the intermolecular complex between Cyt *f* and Pc, both from spinach. The structure of the reduced Pc was determined using high field NMR spectroscopy, whereas the structure of oxidized Cyt *f* was obtained by homology modeling calculations and molecular dynamics. The structure of the intermolecular Cyt *f*-Pc complex was derived using a docking genetic algorithm that takes into account biological information obtained from mutagenesis experiments. Finally, the most relevant structure-based electron transfer pathways from the heme group of Cyt *f* to the copper ion of Pc were calculated based on a model that analyzes the process of electron tunneling between the redox partners in terms of the contributions of covalent bonds and H-bonds and through-space contributions (33–35). In the absence of any direct structural characterization of the Pc-Cyt *f* complex, the information provided by our study is valuable as a structural model for the interpretation of experimental data for this system.

EXPERIMENTAL PROCEDURES

Plastocyanin Sample Preparation—Plastocyanin extraction from 1.5 kg of spinach leaves was carried out by homogenizing the leaves, previously rinsed with distilled water, in 3 liters of 10 mM potassium phosphate buffer, pH 7, containing 50% acetone (v/v) using a Waring blender and keeping the homogenate at 4 °C for 30 min. The undissolved material was removed by centrifugation (5000 × *g*). Protein precipitation was carried out by slowly adding cold (−20 °C) acetone (up to 75%) to the clear supernatant. The pellet obtained after centrifugation was redissolved in 20 mM potassium phosphate buffer, pH 7. The subsequent purification procedure was adapted from a previously published method (36, 37) modified by adding a final hydrophobic interaction chromatographic step on a Toyopearl HW-65C column. Pc was eluted using a linear gradient (60–20%) of ammonium sulfate and finally dialyzed. The purity and concentration of the protein were monitored using a CARY-3 UV-visible spectrophotometer. The absorbance ratio A_{278}/A_{597} for the purified oxidized Pc was 1.15. The protein concentration was determined using a value of 4.9 mM^{-1} cm^{-1} for the extinction coefficient of oxidized Pc at 597 nm (36). Samples for NMR spectroscopy (1–2 mM) were prepared in 50 mM sodium phosphate buffer (either in 90% H_2O, 10% D_2O or in 100% D_2O) at pH 7.5. Complete reduction of the protein was obtained by the addition of a slight excess of a freshly prepared sodium ascorbate solution. During

the NMR experiments, the sample was kept under argon.

NMR Spectroscopy Data Acquisition and Processing—NMR experiments were performed on Bruker Avance spectrometers operating at 500- and 800-MHz proton Larmor frequencies. Data acquisition and processing were performed using a standard Bruker software package (XWINNMR).

Two-dimensional ^{1}H homonuclear TOCSY (38–41) and NOESY (38, 42, 43) experiments were acquired at 293, 295, and 298 K in-phase sensitive time proportional phase increment mode (44, 45) using unlabeled Pc. Water suppression was achieved with a WATERGATE sequence (46). The spin-lock time in TOCSY experiments was varied between 30 and 70 ms, whereas the mixing time used in NOESY was 100 ms. The repetition time in two-dimensional spectra ranged between 1.2 and 1.7 s. Two-dimensional ^{1}H homonuclear TOCSY and NOESY spectra consisted of 4096 K data points in the F2 dimension, whereas 800–1024 experiments were recorded in the F1 dimension with 32–128 transients/experiment. Raw data were processed using a sine-squared window function shifted by either $\pi/2$ or $\pi/3$ in both dimensions. A polynomial base-line correction was applied in both directions. Data were always zero-filled in the F1 dimension to obtain matrices with 2 × 2-K data points. The spectra were calibrated assigning a chemical shift of 4.81 ppm to the water signal with respect to 2,2-dimethyl-2-silapentanesulfonic acid at 291 K.

Peak Assignment and Structural Constraints—The program XEASY (47) was employed for spectral analysis and for NOESY cross-peak integration. The sequence-specific resonance assignment was carried out using standard procedures. The volumes of assigned NOESY cross-peaks were transformed into ^{1}H-^{1}H upper distance limits using the program CALIBA (48). Standard calibration was performed using backbone, side-chain, and methyl classes using a $(1/r)^6$ distance dependence. Dihedral ϕ and ψ angle constraints were obtained from the relative intensities of the intraresidue and interresidue Hα-NH NOESY cross-peaks. All of the dihedral angles constraints (47 ϕ and 47 ψ angles) were divided into two classes. For $^3J_{H\alpha\text{-}NH}$ constants larger than 8 Hz, the ϕ dihedral angle was restrained between −145 and −75° and the ψ angle was restrained between −70 and 0° (region B of the Ramachandran plot), whereas for coupling constants smaller than 4.5 Hz, the ϕ angles were restrained between −105 and −35° and the ψ angles were restrained between 100 and 180° (region A of the Ramachandran plot).

Additional 20 constraints were introduced by considering the presence of H-bonds involving peptide amide NH groups and carbonyl oxygen atoms. Such constraints were considered only in cases where the amide ^{1}H resonance was observed to be non-exchanging in 90% D_2O solutions after 10 min and if the H-bond involving this proton was observed in >50% of the structures calculated using DYANA (49) (see below) without inclusion of these constraints. For these cases, the upper and lower distance limits used for the H–O distance were 1.8 and 2.4 Å, respectively. Moreover, the N–O distances were constrained between 2.4 and 3.4 Å.

The copper atom was included in the structure calculations as a residue bound to the C terminus of the protein by 33 linker dummy residues using the procedure implemented in DYANA (49). These dummy residues are used to let the copper atom move freely during the DYANA run. The number of these residues in the linker is chosen to be large enough to allow the copper atom to get close to any residue in the protein according to the experimental constraints relative to the copper ion. Bond distance restraints were imposed to the copper coordination using lower and upper distance limits, large enough to allow the metal-bound residues to adopt a conformation in solution that would be consistent with the rest of NMR data. In particular, the restraints of 2.0 ± 0.3 and 2.2 ± 0.3, corresponding to normal coordination bonds, were used for Cu-N(His) and Cu-S(Cys), respectively, on account of the large contact interaction experienced by these ligands. The Cu-S(Met) distance was freely allowed to vary within a larger range (from 2.4 to 3.2 Å) to account for the much smaller contact contribution experienced by this residue. No copper-ligand angle restraints were used at this stage of the calculation.

NMR Structure Calculation—Structures were calculated by simulated annealing torsion angle dynamics carried out using DYANA. The calculations started from 400 randomly produced conformers, each of them subjected to 8000 torsion angle dynamics steps in order to adapt its conformation to the distance constraints. The stereospecific assignments (37 in total) were obtained using GLOMSA. Few cycles of (i) structure calculation and (ii) re-calibration using CALIBA allowed the obtainment of an ensemble of structures satisfying the experimental constraints. The best 30 structures having a target function smaller than 0.84 Å^2 were selected as a single family to assess the structure quality and for further analysis.

NMR Structure Refinement—The mean structure from the DYANA family was calculated using MOLMOL and subjected to restrained energy minimization using the SANDER module of the AMBER 6.0 program package. The force-field parameters for all of the residues excluding those for the copper-coordinated ligands were the standard AMBER "all-atoms" parameters. The calculations were performed *in vacuo* with the distance-dependent dielectric constant option. The non-bonded interactions were evaluated with a cutoff of 10 Å. The mixed linear-harmonic flat-bottomed potential implemented in SANDER was applied to all of the structural constraints. This potential involves a null force constant for structural constraints within the allowed limits, a non-zero harmonic force constant in a small interval outside the allowed limits, and a linearly dependent potential beyond that limit. Nuclear Overhauser effect-derived distance constraints were restricted below the upper distance limit (r_i) using a force constant of 32 kcal mol^{-1} Å^{-2} for the interval r_i + 0.5 Å. Distance constraints involving the same H-bonds used for DYANA calculations were included in the restrained energy minimization calculation, restricting the NH–O and N–O distances to the same upper (r_i) values used in DYANA with a force constant of 32 kcal mol^{-1} Å^{-2} for the range of r_i + 0.5 Å. The Cu-N(His) and Cu-S(Cys) distances were constrained at 2.1 ± 0.1 and 2.2 ± 0.1, respectively, using a linear-harmonic flat-bottomed potential with force constants of 50 kcal mol^{-1} Å^{-2} in the 0.3-Å distance ranges below and above these limits. The Cu-S(Met) distance was analogously constrained within the 2.75 ± 0.05-Å range using a force constant of 40 kcal mol^{-1} Å^{-2}. The Cu-N(His)-C, Cu-N(His)-C, Cu-S(Cys)-C, Cu-S(Met)-C, and Cu-S(Met)-C angles were restrained around 127 ± 10, 127 ± 10, 105 ± 5, 130 ± 10, and 110 ± 10, respectively, using a linear-harmonic flat-bottomed potential with force constants of 50 kcal mol^{-1} deg^{-2} in the 50 ranges below and above the given values. Analogously, the (His)N-Cu-N(His), (His)N-Cu-S(Cys), (His)N-Cu-S(Met), and (Met)S-Cu-S(Cys) angles were restrained in the 110 ± 10, 125 ± 10, 95 ± 10, and 100 ± 10 range with a force constant of 20 kcal mol^{-1} deg^{-2} in the 50 angle ranges below and above these limits.

The mean minimized structure of reduced spinach Pc was subsequently subjected to molecular dynamics calculation in a box of 72 × 70 × 67 Å filled with TIP3P water molecules (50). The water molecules were equilibrated for 100 ps at the temperature of 300 K using the SANDER module of AMBER 6 program (51). After this step of solvent equilibration, the model underwent 400 ps of constrained molecular dynamics at 300 K and to 3000 steps of energy minimization. The force-field parameter for the copper center was taken as previously described (52).

Determination and Refinement of the Model Structure of Spinach Cytochrome f—The sequence of spinach apocytochrome *f* precursor (53, 54) was retrieved from the Swiss-Prot Data Base available at expasy.org/sprot/. An initial homology model of spinach Cyt *f* was obtained using the server SWISS-MODEL (55, 56) available at swissmodel.expasy.org. The server automatically (i) searches for template structures using the program BLAST2 (57); (ii) selects all of the templates with sequence identities above 25% and projected model size larger than 20 residues using the program SIM (58); (iii) generates all of the models using the program ProMod II (55); and (iv) minimizes all of the models using the program GROMOS96 (59). The output of this procedure is represented by the best model obtained on the basis of a calculated B-factor that takes into account the following: (i) the number of template structures used for model building; (ii) the deviation of the models from the template structures; and (iii) the distance trap value used for framework building. The heme group and the vicinal structurally conserved internal chain of water molecules (60) were inserted in the model by superimposition with the highest resolution crystal structure of turnip Cyt *f* (Protein Data Bank code 1HCZ).

The initially obtained model was subsequently inserted in a box of 115 × 65 × 62 Å filled with TIP3P water molecules (50). The water molecules were equilibrated for 100 ps at the temperature of 300 K using the SANDER module of the AMBER 6 program (51). After this step of solvent equilibration, the model was subjected to 400 ps of molecular dynamics at 300 K and to 3000 steps of energy minimization. The force-field parameter for the oxidized *c*-type heme group of Cyt *f* was taken from previously available data (61). The final structural model of oxidized spinach Cyt *f* was validated using the programs PROCHECK (62) and PROSA II (63).

Determination of the Structure of Intermolecular Complex between Plastocyanin and Cyt f—The model of the transient complex between spinach Pc and Cyt *f* was calculated using the program AUTODOCK3 (64) with the Cyt *f* as the receptor. The plastocyanin molecule was allowed to move in a cubic box large enough (47-Å edge) to allow free rotation of the Pc molecule and placed on the surface of Cyt *f* in the

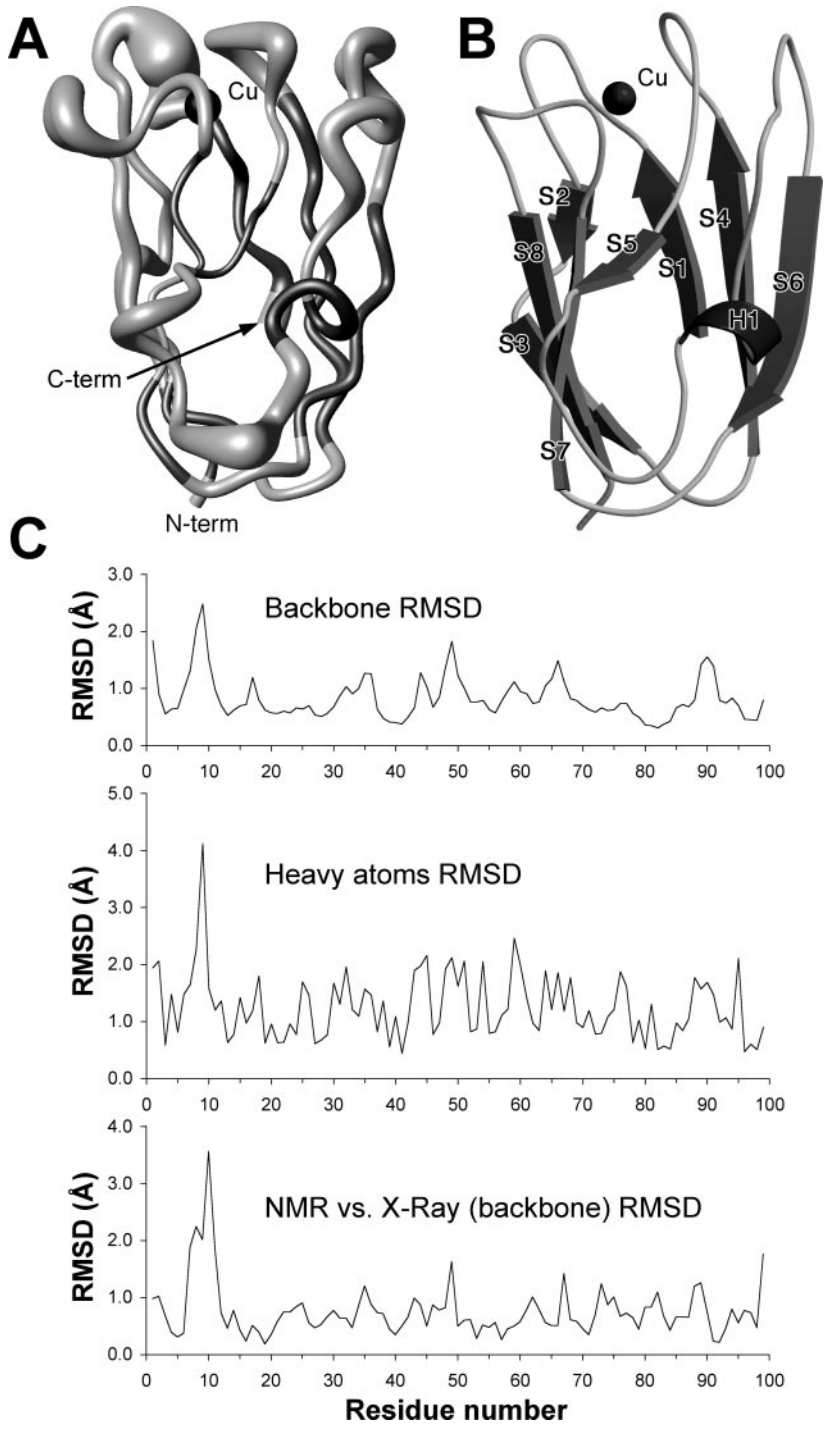

FIG. 2. *A*, "sausage" diagram of the superimposed 20 DYANA backbone structures of reduced spinach leaves Pc as determined by NMR. *B*, ribbon diagram of native spinach Pc-minimized mean structure revealing the position of the copper center and the sequence-specific secondary structure. *C*, plot of the global backbone and heavy atoms pairwise per residue for the 20 structures family as well as the backbone r.m.s.d. between the mean minimized NMR structure of native spinach Pc and the x-ray structure of the mutant spinach Pc. The copper ion is shown as a *black sphere* of arbitrary radius.

heme region near the smaller domain. The electrostatic potential grid of this cubic box was calculated using a grid spacing of 0.375 Å. The Lamarckian genetic algorithm was used to perform 5000 simulations. Step sizes of 2 Å for translation and 50° for rotation were chosen, and the maximum number of energy evaluations was set to 250,000. For each of the 5000 independent runs, a maximum number of 27,000 genetic algorithm operations were generated on a single population of 50 individuals. Operator weights used for cross-over, mutation, and elitism were default parameters (0.80, 0.02, and 1, respectively). The best complex was chosen as the result of two subsequent filtering operations. First, the conformers with Fe-Cu distance larger than 20 Å were considered as inappropriate and thus were discarded. Secondly, the remaining models were filtered by using a score parameter that takes into account the following: (i) the Fe-Cu distance; (ii) the distance between the Cα atoms of the residues in the hydrophobic region of Pc and the residues in the heme region of Cyt *f*; and (iii) the distance between the Cα atoms of the residues in the acidic patch of Pc and the residues in the basic patch on Cyt *f*. The side chains of the best complex satisfying the above criteria were subjected to 1000 steps of energy minimization using the SANDER module of the AMBER 6 program (50). The coordinates of the structure of reduced spinach Pc have been deposited in the Protein Data Bank (code 1YLB), whereas the models for the oxidized spinach Cyt *f* and spinach Pc-Cyt *f* complex have been deposited in the www.postgenomicnmr.net protein data base.

The donor-acceptor interaction associated with electron tunneling and the electron transfer path between reduced Pc and oxidized Cyt *f* were calculated using the PATHWAYS module of the program HARLEM (65) applied to the energy minimized model of the Pc-Cyt *f* complex.

RESULTS AND DISCUSSION

Spinach Plastocyanin NMR Structure Determination—The obtained ^{1}H NMR signal assignment for reduced native spin-

TABLE I
Restraint violations and structural and energetic statistics for the solution structure of reduced plastocyanin from spinach leaves

	Mean structure
RMS violations per experimental distance constraint (nm)	
Intraresidue (223)[a,b]	0.0057
Sequential (342)	0.0059
Medium range (179)	0.0188
Long range (638)	0.0162
Total (1382)	0.0135
Φ angle constraints (47)[c]	3.2726
Ψ angle constraints (47)[c]	4.9751
Average number of violations per structure	
Intraresidue	1
Sequential	2
Medium range	3
Long range	13
Total	19
Φ angle	3
Ψ angle	3
Violations larger than 3 nm	0
Violations between 1 and 3 nm	7
Target function (nm^2)	58
AMBER forcefield average total energy ($kJ \cdot mol^{-1}$)	−1134
Structure analysis	
% residues in most favored regions	84.8
% residues in allowed regions	13.9
% residues in generally allowed regions	
% residues in disallowed regions	1.3
No. of bad contacts/100 residues[d]	0.0
H-bond energy ($kJ \cdot mol^{-1}$)[d]	0.8
Overall G-factor[d]	−0.36
Z-score (PROSA II)	−10.09

[a] The number of meaningful constraints for each class is reported in parentheses.
[b] Medium-range distance constraints are those among residues (i, i + 2), (i, i + 3), (i, i + 4), and (i, i + 5).
[c] In degrees.
[d] The programs PROCHECK and PROCHECKNMR were used to check the overall quality of the structure. For the PROCHECK statistic, <10 bad contacts/100 residues, an average hydrogen bond energy in the range of 2.5–4.0 $kJ \cdot mol^{-1}$ and an overall G-factor larger than −0.5 are expected for a good quality structure.

ach Pc (Supplemental Table I), a prerequisite for determination of protein solution structure, extends and improves a previously reported partial assignment (66). The few proton signals remaining unassigned are either heavily overlapped or experience exchange phenomena that prevent their observation. The NMR experimental data used for structure calculation are reported in Supplemental Table I, whereas Supplemental Fig. 1 reports the distribution of the meaningful nuclear Overhauser effects per residue as well as the residue-by-residue experimental constraints used for the structure calculation.

The 20 structures generated by torsion angle dynamics calculations and having the lowest target function (≤0.73 $Å^2$) have no consistent violations, have no residual violation exceeding 0.3 Å, and experience mean global r.m.s.d. values of 0.99 ± 0.13 and 1.48 ± 0.14 Å for the backbone and heavy atoms, respectively. A "sausage view" of the backbone atoms of the DYANA family is shown in Fig. 2*A*, whereas the average structure obtained after restrained energy minimization and dynamics in explicit water is shown in Fig. 2*B*. The distribution of the final r.m.s.d. per residue within the family is reported in Fig. 2*C*. The final structure quality parameters of the structure subjected to molecular dynamics in water are reported in Table I.

The large number of experimental NMR constraints for the reduced spinach Pc provides a well ordered protein family. The characteristics determined for the final calculated structures of the protein (Table I) indicate that the structure completely fits the experimentally determined NMR geometric constraints. From the analysis of the r.m.s.d. per residue distribution (Fig. 2*C*) as well as the ensemble sausage view (Fig. 2*A*), it can be concluded that the family is generally well ordered with the exception of the loops located close to the copper center and on the opposite side of the protein. It has been reported that the regions near the copper ion are characterized by increased flexibility on the long time scales (52, 67). A comparison of the r.m.s.d. per residue for reduced spinach Pc and reduced *Synechocystis* sp. PCC 6803 Pc (52) reveals a large similarity. The peak backbone r.m.s.d. value in the case of spinach Pc was found for Asp^9 (2.48 Å). This residue is next to Gly^8, which appeared to be too mobile to allow native protein crystallization, and indeed a G8D substitution resulted in the crystallization of the mutant protein and subsequent structure determination (68). As a result of this flexibility, Gly^8 has only very few nuclear Overhauser effect constraints, in turn, reflected on the decreased family resolution around Gly^8 and Asp^9.

All of the Pcs feature rather similar secondary and tertiary structures despite significant sequence variability. The structure of reduced spinach Pc obtained after molecular dynamics in water is composed of eight β-strands organized in two twisted sheets. The first β-sheet is composed of three strands formed by residues Val^1-Leu^5 (strand S1), Phe^{14}-Leu^{15} (strand S2), Glu^{25}-Asn^{31} (strand S4), and Thr^{69}-Leu^{74} (strand S6). The β-strands involving residues Gly^{17}-Val^{21} (strand S3), Val^{40}-Phe^{41} (strand S5), Thr^{79}-Tyr^{83} (strand S7), and Val^{93}-Thr^{97} (strand S8) constitute the second β-sheet. Both β-sheets have mixed parallel and antiparallel strands connected by several turns and loops. Moreover, the protein has a short 3_{10} helix (H1) that comprises three residues (Ala^{52}-Lys^{54}). The protein does not have any other regular secondary structure in addition to the mentioned structural motifs.

A comparison of the NMR solution structure of the native spinach Pc with the x-ray solid-state structure of the mutant protein (68) reveals a substantial conformational similarity. The r.m.s.d. per residue (average value = 0.89 Å) shown in Fig. 2*C* indicates that these values are smaller than the r.m.s.d. of the NMR structure family; therefore the observed differences do not have statistical significance. As expected, the most pronounced structural variations are found in the four loops located near the copper center, in particular in the region around the mutated Gly^8.

Spinach Cytochrome f Model Structure Calculation—Fig. 3 reports the multiple sequence alignment of the spinach apocytochrome *f* precursor with Cyt *f* from turnip, *C. reinhardtii*, and *P. laminosum* (sequence identity of 91.3, 68.2, and 62.2% respectively) whose crystal structures are available (Protein Data Bank codes 1HCZ, 1CFM, and 1CI3, respectively). The backbone r.m.s. deviations of these three proteins are in the range of 0.7–0.8 Å indicating a substantial structural similarity despite the different biological source. These three structures were used for spinach Cyt *f* model calculations using homology building. The structures of the Cyt *f* in the full b_6f complexes were not used for model building because of their much lower resolution (3.1 and 3.0 Å for 1Q90 and 1VF5, respectively) than found for the soluble Cyt *f* domains (1.9–2.0-Å range). In addition, the low backbone r.m.s.d. values between the soluble and membrane-bound domains (0.6–1.2 Å) suggest that the inclusion of the full complex structures is not necessary.

The calculated structure of the spinach Cyt *f* is shown in Fig. 4*A*. The analysis of the Ramachandran plot reveals that 83.4% residues reside in the most favored regions, 16.1% in the allowed regions, and 0.5% in the generously allowed regions. No residues were found in disallowed regions, indicating the high

```
                                    1       10        20        30        40        50        60        70        80
                                    |       |         |         |         |         |         |         |         |
SPIN  MQTINTFSWIKEQITRSISISLILYIITRSSIANAYPIFAQQGYENPREATGRIVCANCHLANKPVDIEVPQAVLPDTVFEAVVRIPYDMQLKQVLANGKKGGLNVGAVLILPEGFELAP 85
CREI  ------------------------------------YPIFAQQNYENPREATGRIVCANCHLASKPVDIEVPQAVLPDTVFEAVVKIPYDMQLKQVLANGKKGALNVGAVLILPEGFELAP 85
PLAM  ------------------------------------YPFWAQQNYANPREATGRIVCANCHLAAKPAEIEVPQAVLPDSVFKAVVKIPYDHSVQQVQADGSKGPLNVGAVLMLPEGFTIAP 85
TURN  ------------------------------------YPIFAQQNYENPREATGRIVCANCHLASKPVDIEVPQAVLPDTVFEAVVKIPYDMQLKQVLANGKKGALNVGAVLILPEGFELAP 85

          90        100       110       120       130       140       150       160       170       180       190       200
          |         |         |         |         |         |         |         |         |         |         |         |
SPIN  PDRISPEMKEKMG-NLSFQSYRPNKQNILVIGPVPGQKYSEITFPILAPDPATKKDVHFLKYPIYVGGNRGRGQIYPDGSKSNNTVYNSTATGIVKKIVRKEKGGYEINIADASDGREVV 204
CREI  PDRISPEMKEKIG-NLSFQNYRPNKKNILVIGPVPGQKYSEITFPILAPDPATNKDVHFLKYPIYVGGNRGRGQIYPDGSKSNNTVYNATAGGIISKILRKEKGGYEITIVDASNERQVI 204
PLAM  EDRIPEEMKEEVGPSYLFQPYADDKQNIVLVGPLPGDEYEEIVFPVLSPNPATNKSVAFGKYSIHLGANRGRGQIYPTGEKSNNAVYNASAAGVITAIAKADDGSAEVKIR-TEDGTTIV 204
TURN  PDRISPEMKEKIG-NLSFQNYRPNKKNILVIGPVPGQKYSEITFPILAPDPATNKDVHFLKYPIYVGGNRGRGQIYPDGSKSNNTVYNATAGGIISKILRKEKGGYEITIVDASNERQVI 204

          210       220       230       240       250 252
          |         |         |         |         | |
SPIN  DIIPRGPELLVSEGESIKLDQPLTSNPNVGGFGQGDAEVVLQDPLRIQGLLFFFASVILAQIFLVLKKKQFEKVQLSEMNF 252
CREI  DIIPRGLELLVSEGESIKLDQPLTSNPNVGGFGQGDAEIVLQDPLR---------------------------------- 250
PLAM  DKIPAGPELIVSEGEEVAAGAALTNNPNVGGFGQKDTEIVLQSPN---------------------------------- 249
TURN  DIIPRGLELLVSEGESIKLDQPLTSNPNVGGFGQGDAEIVLQDPLRVQ---------------------------------- 252
```

FIG. 3. **Multiple sequence alignment of spinach leaves apocytochrome *f* (*SPIN*), native *C. reinhardtii* Cyt *f* (*CREI*), native *P. laminosum* Cyt *f* (*PLAM*), and native turnip Cyt *f* (*TURN*).** Non-modeled residues are reported in *italics*. Conserved residues are in *boldface*, whereas heme-bound cysteines are *underlined* and axial ligands are highlighted in *gray*.

quality of the Cyt *f* model. This is further confirmed by the analysis performed using the program PROSA, which resulted in a *Z*-score value of −10.09.

The overall backbone r.m.s.d. between the calculated structure of spinach Cyt *f* and the structures used as templates is in the range of 1.42 and 1.48 Å, which indicates an overall large similarity. This is evidenced in Fig. 4*B*, which reveals that the major difference is represented by the slightly perturbed conformation of the long linker between the small and the large domains.

Spinach Cyt f-Pc-calculated Complex—The structures of spinach Pc and Cyt *f* obtained by NMR and molecular modeling, respectively, were utilized to calculate a structure of their complex that best adheres to the chosen criteria, which involve mainly short distances between the redox centers and between the protein patches known to be involved in the complex.

Fig. 5*A* highlights the orientation assumed by the two proteins in the model complex, whereas Fig. 5*B* highlights their shape complementarity, which results in a total interface area of 835 Å^2. In the calculated model, the acidic patch of Pc is found close to the basic patch on Cyt *f*. In particular, residues Asp^{42} and Glu^{43} of Pc are in close contact (any interatomic distance <4 Å) with Cyt *f* residues Arg^{209} and Lys^{65}, whereas residues Asp^{44} and Glu^{45} of Pc are close to Cyt *f* Lys^{187}. Residue Glu^{59} on the acidic region of Pc is in close proximity to Cyt *f* Lys^{66}. The interactions between the hydrophobic patches on the two proteins involve residues 12, 35, 36, 40, 83, and 85–90 on Pc and 1, 3, 4, 61–63, 156, 160, 161, and the heme group on Cyt *f*.

The mode of interaction between Pc and Cyt *f* in the model calculated in the present study is largely similar to the complex previously proposed for the turnip Cyt *f* and spinach Pc based on NMR data (22). This similarity is evident upon superposition of the two structures, which results in the Pc chain in the spinach homologous complex falling within the ensemble of 10 Pc chains that best satisfy the NMR constraints in the heterologous higher plant complex. In particular, it is evident how the Pc chain adheres to the Cyt *f* in a side-on fashion as opposed to the homologous cyanobacterial complex for which a head-on interaction is found (31, 32). The model also reproduces most of the structural features at the interface found for the heterologous complex between turnip Cyt *f* and spinach Pc (22) with similar complementary acidic/basic and hydrophobic patches involved in the interaction (Fig. 5*C*).

In the present model, the shortest distance between the two proteins involve the copper-binding residue His^{87} of Pc and the heme ligand Tyr^1 (4.2 Å between His^{87} Nϵ and Cyt *f* Tyr^1 Cδ2, Fig. 6*A*). The Cu-Fe distance, 12.2 Å, is slightly larger than in the NMR-calculated complex (10.7–11.3 Å) (22) but is much shorter than the distance found in the same complex generated using molecular dynamics (14 Å) (19). In the case of the complex obtained manually taking into consideration electrostatic interactions, no indication is given for the Cu-Fe distance or for the electron transfer pathway (17). No comparison is possible between our model and the models determined either manually or by molecular dynamics simulations because of the unavailability of the latter structures in Protein Data Bank format.

The best electron transfer pathway calculated using the program HARLEM involve Cyt *f* Tyr^1 and Pc His^{87} (Fig. 6*A*) for

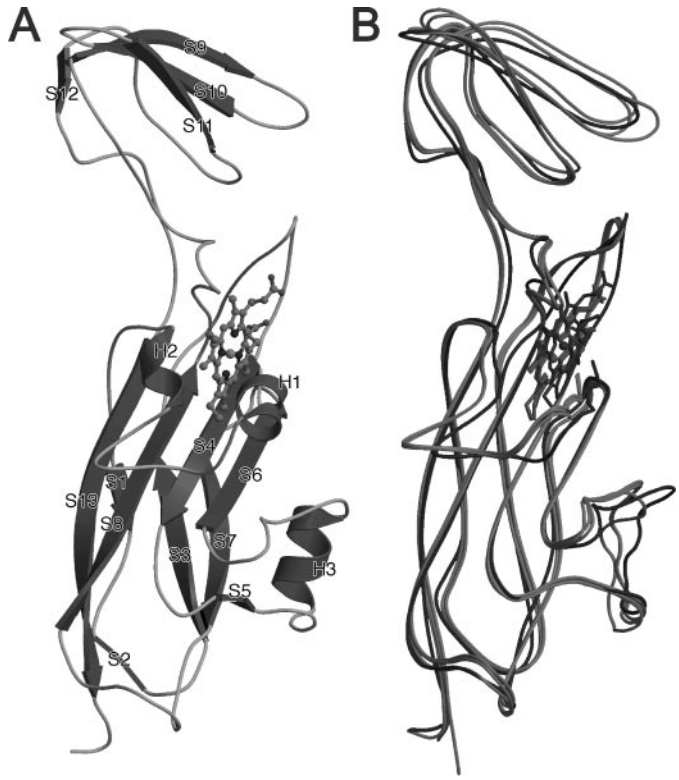

FIG. 4. *A*, ribbon diagram of the calculated model for spinach Cyt *f* revealing the position of the heme group shown in *ball-and-stick* and the secondary structure elements. *B*, superimposition of the backbone of the calculated model for spinach Cyt *f* (*black*) with the template crystal structures used for the homology building (*gray*). The metal ions are shown as *black spheres* of arbitrary radius.

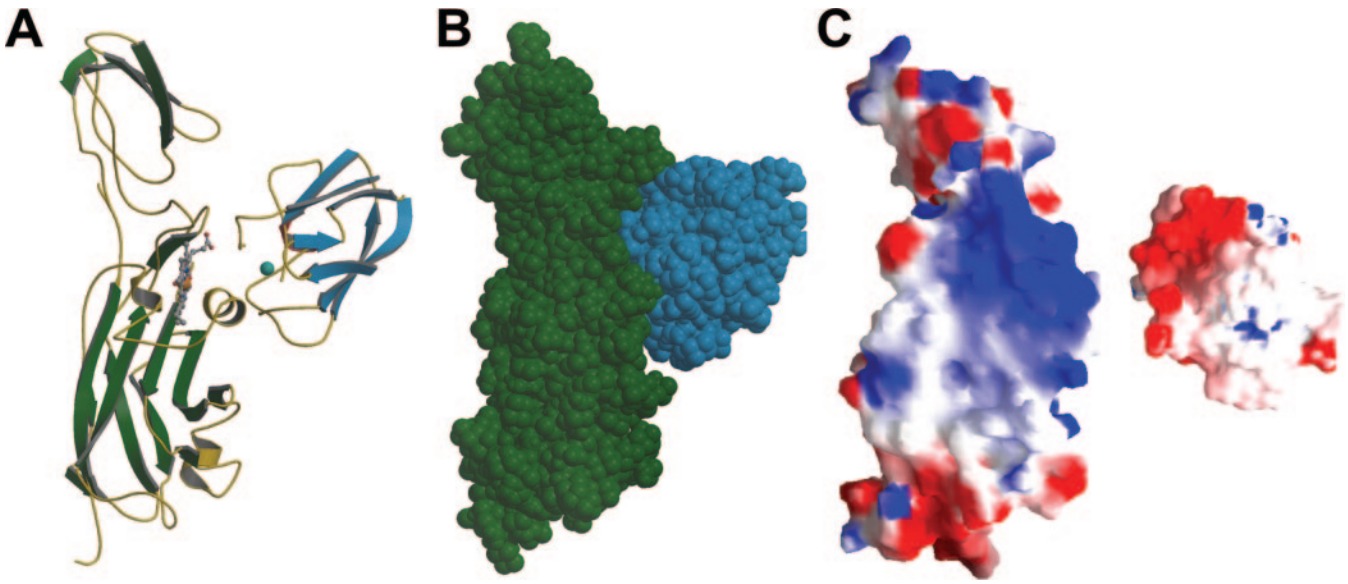

FIG. 5. Ribbon (*A*) and spacefill (*B*) representation of spinach Cyt *f*-Pc model complex is shown. Cyt *f* β-strands and spacefill are *green*, while in Pc they are *cyan*. Cyt *f* and Pc helices are colored in *yellow* and in *red*, respectively. Heme group and copper ion are reported in *ball-and-stick* representation. Color scheme: β-strands, *green*; helix, *yellow*; C atom, *gray*; N atom, *blue*; O atom, *red*; S atom, *yellow*; iron atom, *orange*; and copper atom, *cyan*. *C*, GRASP solid surface representation of the electrostatic potential calculated separately for spinach Cyt *f* and Pc. The proteins are shown rotated by +90 and −90°, respectively, as compared with *panels A* and *B* with the protein interaction surface positioned toward the viewer. The surface is colored according to the calculated electrostatic potential contoured from −5.0 *kT*/e (*intense red*) to +5.0 (where k = Boltzmann constant, T = absolute temperature, and e = electron charge) (*intense blue*).

which the coupling decay value[2] is 1.8×10^{-4}. This value is comparable, for example, with the value found for fast intramolecular electron transfer in multi-heme cytochromes (70). The electron transfer coupling decay from the heme to any specific point on the surface of the two proteins in the complex is reported in Fig. 6*B*. This calculation provides a qualitative idea of the electron transfer properties of the two protein surfaces in the complex and is consistent with the electrons flowing most probably from the heme iron ion of Cyt *f* to the copper ion of Pc using the surface patches that were independently calculated as involved in the interaction. This result also indicates that the calculated best model may not represent the only specific structure for which the redox reaction occurs but rather that multiple possible associations with different electron transfer capabilities may exist both *in vitro* and *in vivo*. This is important especially if one considers that *in vivo* the luminal volume may regulate the way the two proteins approach and dock. The determined mapping of the predicted coupling decay values on the surface of the two proteins is helpful in widening the possibilities for electron transfer to occur *in vivo*.

At this point, it is worthwhile considering possible mechanisms of interaction and electron transfer between membrane-embedded pigment-protein complexes and small soluble proteins. Comparative kinetic analysis of electron transfer between redox carriers in a variety of evolutionarily differentiated organisms made it possible to put forward different reaction mechanisms for PS I reduction/Cyt b_6f complex oxidation by Pc (for review, see Ref. 3). These mechanisms include the following: a simple bimolecular collision (type I); a two-step mechanism involving complex formation prior to the electron transfer (type II); and a three-step mechanism involving a rate-limiting conformational change within the complex before intracomplex electron transfer (type III) (71). The type III mechanism implies that the donor and acceptor proteins form a complex in which, for some reasons, the probability of electron transfer is low. The internal fast electron transfer occurs after rearrangement of the complex to a favorable configuration. It is likely that the type III mechanism may function in all of the cases, whereas the observed kinetics can be described by the other mechanisms because of the relative speeds of the electron transfer or rearrangement steps (3). This suggestion, in the case of PS I reduction by Pc, was supported by experimental results obtained by direct electrometric technique (72).

The complex formation between proteins is a multi-step process. Initially, the encounter complex is formed in which electrostatic interactions are dominant. It was suggested that the reaction rate, but not the structure of the complex, may depend on electrostatics (73). Finally, a well defined complex is formed in which electron transfer can occur.

The interaction between Cyt *f* and Pc is highly transient. The lifetime of ~100 μs was estimated for the final specific complex (73). Within this lifetime window, the proteins have to form a specific complex and transfer an electron. The first order rate constants experimentally obtained for the electron transfer between Cyt *f* and Pc from the higher plants are in the range of $2 \div 7 \times 10^{-4}$ s^{-1} (see Refs. 16 and 74). This range of rate constants is consistent with the coupling decay value derived from the spinach Cyt *f*-Pc-calculated complex, corresponding to the Cu-Fe distance of 12.2 Å.

According to its function as electron carrier between Cyt b_6f and PS I, Pc forms complexes with the two membrane-

[2] The coupling decay value is a unitless parameter related to the electronic coupling between the donor (*D*) and the acceptor (*A*) center. The electronic coupling is the T_{DA} parameter included in the Marcus equation describing the extent of wave function overlap between the donor and acceptor centers,

$$k_{ET} = \left(\frac{\pi}{\hbar^2 \lambda k_B T}\right)^{1/2} [T_{DA}]^2 \exp\left\{-\left[\frac{(\Delta G^\circ + \lambda)^2}{4\lambda k_B T}\right]\right\}$$

where k_{ET} is the electron transfer rate constant, λ is the nuclear reorganization energy, k_B is the Boltzmann constant, T is the absolute temperature, and ΔG° is the driving force related to the difference in reduction potential between the donor and acceptor. The coupling decay is calculated in the pathway model implemented in HARLEM as the product of distinct parameters for the electronic coupling mediated by: (i) covalent bonds; (ii) hydrogen bonds; and (iii) through-space interactions. The larger the value of the coupling decay constant, the shorter and more efficient the pathway is from donor to acceptor because of the larger electronic coupling.

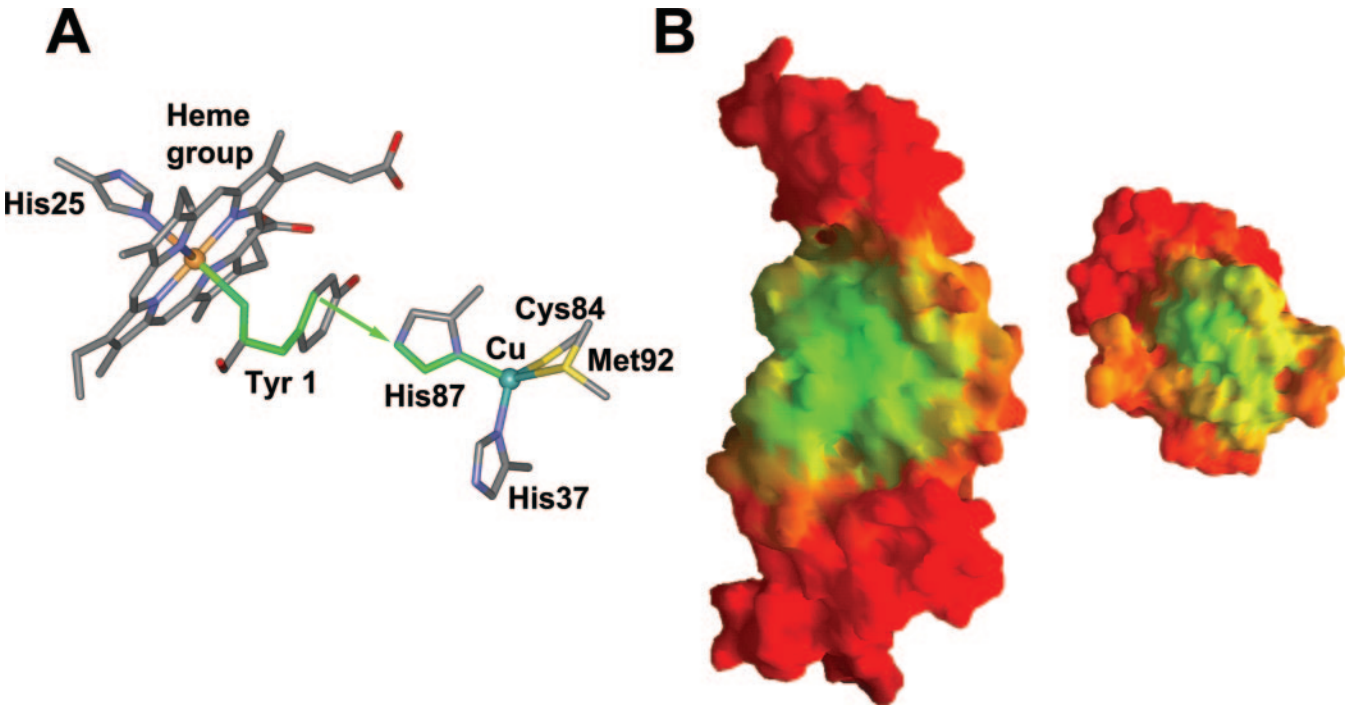

FIG. 6. *A*, stick diagram revealing the details of the complex interface (Cyt *f*, *green*; Pc, *cyan*; iron, *orange*; and copper, *cyan*). The best electron transfer pathway is highlighted as *thick bonds* and *red lines*. *B*, GRASP solid surface representation of the electron transfer coupling decay calculated for the complex between spinach Cyt *f* and Pc. The proteins are shown rotated by +90 and −90°, respectively, as compared with Fig. 5, *A* and *B*, with the protein interaction surface positioned toward the viewer. *Green-colored zones* correspond to high coupling decay values for electron transfer from the donor heme group. The range spans from −20 (*red*) to −10 (*yellow*) to 0 (*green*) in ln(coupling decay) units as obtained from HARLEM.

anchored proteins. On the basis of the large efficiency of the cyclic electron flow observed in spinach leaf, it was recently suggested that a significant fraction of Pc molecules is organized in supercomplexes that associate one Cyt b_6f complex, one PS I, one Pc, and one ferredoxin molecule (75). These supercomplexes were proposed to be the units where the cyclic electron flow operates. The formation of a similar supercomplex between Cyt b_6f and PS I complexes involving Cyt c_6 in the hybrid proteoliposomes was proposed to explain the high rate of the flash-induced electron transfer measured by direct electrometrical technique in this model system (76).

However, our preliminary results of comparison of the Pc orientation in electron transfer complexes with the Cyt b_6f and PS I complexes showed that the formation of the supercomplex was fairly improbable (data not shown). Although the docking sites of Pc interaction with Cyt b_6f and PS I are not similar, they are rather close to one another. It can be obseved that (i) the acidic area on Pc recognizes a series of basic amino acid residues at the N terminus of the PS I PsaF subunit, and almost the same area interacts with the positively charged residues of the Cyt *f* subunit, (ii) the complex at PS I incorporates the whole hydrophobic surface of Pc (between Gly^{10} and Ala^{90}), whereas the complex between Pc and Cyt *f* involves the protein patch around Ala^{90}, and (iii) the two electron transfer pathways involve the Pc copper ligand, His^{87} (see Refs. 3, 77, and 78 and references therein).

To explain the experimental data indicating the supercomplex formation and the structural data on the overlapping docking sites of Pc-Cyt *f* and Pc-PS I complexes, it is safe to suggest the following.

(i) Diffusion of soluble Pc occurs not in three-dimensions but is limited by some attractive interaction to the membrane interface (*i.e.* is a two-dimensional diffusion), leading to a considerably increased rate of reaction of soluble components with membrane-embedded pigment-protein complexes. This effect was suggested to explain the interaction of Cyt c_2 with the bacterial reaction centers (79).

(ii) Pc exchanges between Cyt b_6f and PS I via a small local Pc pool in which the rate of exchange between the local and the bulk pools is much slower than the rate of interaction among Cyt b_6f, Pc, and PS I. In other words, Cyt b_6f and PS I may form virtual rather than real supercomplex because the real one implies simultaneous interaction with the same Pc molecule. The existence of the local pools was suggested for the interaction between the Cyt bc_1 complex and the photosynthetic reaction center in chromatophores of purple bacteria (80).

(iii) Oxidized Pc may have lower affinity for PS I and higher affinity for Cyt *f*. Indeed, the tight binding of reduced Pc and a considerably weaker binding of oxidized Pc, which is released from PS I after transfer of an electron to P700, was demonstrated (81).

It is also possible that all of these factors contribute to the fast interaction between Cyt b_6f and PS I, which can be hardly explained by simple collision interaction with Pc. However, further progress in the structural analysis and kinetic experiments is required to provide a deeper insight into the mechanisms of interaction between protein complexes.

Acknowledgments—We thank Prof. Giovanni Venturoli and Dr. Mahir Mamedov for valuable discussions.

REFERENCES

1. Cramer, W. A., Zhang, H., Yan, J., Kurisu, G., and Smith, J. L. (2004) *Biochemistry* **43,** 5921–5929
2. Allen, J. F. (2004) *Trends Plant Sci.* **9,** 130–137
3. Hope, A. B. (2000) *Biochim. Biophys. Acta* **1456,** 5–26
4. Crofts, A. R. (2004) *Annu. Rev. Physiol.* **66,** 689–733
5. Xia, D., Yu, C. A., Kim, H., Xia, J. Z., Kachurin, A. M., Zhang, L., Yu, L., and Deisenhofer, J. (1997) *Science* **277,** 60–66
6. Zhang, Z., Huang, L., Shulmeister, V. M., Chi, Y. I., Kim, K. K., Hung, L. W., Crofts, A. R., Berry, E. A., and Kim, S. H. (1998) *Nature* **392,** 677–684
7. Iwata, S., Lee, J. W., Okada, K., Lee, J. K., Iwata, M., Rasmussen, B., Link, T. A., Ramaswamy, S., and Jap, B. K. (1998) *Science* **281,** 64–71
8. Hunte, C., Koepke, J., Lange, C., Rossmanith, T., and Michel, H. (2000) *Structure Fold Des.* **8,** 669–684
9. Stroebel, D., Choquet, Y., Popot, J. L., and Picot, D. (2003) *Nature* **426,** 413–418

10. Kurisu, G., Zhang, H., Smith, J. L., and Cramer, W. A. (2003) *Science* **302,** 1009–1014
11. Soriano, G. M., Smith, J. L., and Cramer, W. A. (2001) in *Handbook of Metalloproteins* (Messerschmidt, A., Huber, R., Wieghardt, K., and Poulos, T., eds) pp. 172–181, John Wiley & Sons, Inc., New York
12. Martinez, S. E., Huang, D., Szczepaniak, A., Cramer, W. A., and Smith, J. L. (1994) *Structure* **2,** 95–105
13. Carrell, C. J., Schlarb, B. G., Bendall, D. S., Howe, C. J., Cramer, W. A., and Smith, J. L. (1999) *Biochemistry* **38,** 9590–9599
14. Chi, Y. I., Huang, L. S., Zhang, Z., Fernandez-Velasco, J. G., and Berry, E. A. (2000) *Biochemistry* **39,** 7689–7701
15. Freeman, H. C., and Guss, J. M. (2001) in *Handbook of Metalloproteins* (Messerschmidt, A., Huber, R., Wieghardt, K., and Poulos, T., eds) pp. 1153–1169, John Wiley & Sons, Inc., New York
16. Kannt, A., Young, S., and Bendall, D. S. (1996) *Biochim. Biophys. Acta* **1277,** 115–126
17. Pearson, D. C., Jr., Gross, E. L., and David, E. S. (1996) *Biophys. J.* **71,** 64–76
18. Soriano, G. M., Cramer, W. A., and Krishtalik, L. I. (1997) *Biophys. J.* **73,** 3265–3276
19. Ullmann, G. M., Knapp, E.-W., and Kostic, N. M. (1997) *J. Am. Chem. Soc.* **119,** 42–52
20. Pearson, D. C., Jr., and Gross, E. L. (1998) *Biophys. J.* **75,** 2698–2711
21. De Rienzo, F., Gabdoulline, R. R., Menziani, M. C., De Benedetti, P. G., and Wade, R. C. (2001) *Biophys. J.* **81,** 3090–3104
22. Ubbink, M., Ejdeback, M., Karlsson, B. G., and Bendall, D. S. (1998) *Structure* **6,** 323–335
23. Ejdeback, M., Bergkvist, A., Karlsson, B. G., and Ubbink, M. (2000) *Biochemistry* **39,** 5022–5027
24. Bergkvist, A., Ejdeback, M., Ubbink, M., and Karlsson, B. G. (2001) *Protein Sci.* **10,** 2623–2626
25. Lee, B. H., Hibino, T., Takabe, T., and Weisbeek, P. J. (1995) *J. Biochem.* (*Tokyo*) **117,** 1209–1217
26. Gong, X. S., Wen, J. Q., Fisher, N. E., Young, S., Howe, C. J., Bendall, D. S., and Gray, J. C. (2000) *Eur. J. Biochem.* **267,** 3461–3468
27. Gong, X. S., Wen, J. Q., and Gray, J. C. (2000) *Eur. J. Biochem.* **267,** 1732–1742
28. Sykes, A. G. (1991) *Structure Bond.* (*Berlin*) **75,** 177–244
29. Schlarb-Ridley, B. G., Bendall, D. S., and Howe, C. J. (2002) *Biochemistry* **41,** 3279–3285
30. Hart, S. E., Schlarb-Ridley, B. G., Delon, C., Bendall, D. S., and Howe, C. J. (2003) *Biochemistry* **42,** 4829–4836
31. Crowley, P. B., Otting, G., Schlarb-Ridley, B. G., Canters, G. W., and Ubbink, M. (2001) *J. Am. Chem. Soc.* **123,** 10444–10453
32. Crowley, P. B., Vintonenko, N., Bullerjahn, G. S., and Ubbink, M. (2002) *Biochemistry* **41,** 15698–15705
33. Beratan, D. N., Onuchic, J. N., Winkler, J. R., and Gray, H. B. (1992) *Science* **258,** 1740–1741
34. Betts, J. N., Beratan, D. N., and Onuchic, J. N. (1992) *J. Am. Chem. Soc.* **114,** 4043–4046
35. Beratan, D., and Skourtis, S. (1998) *Curr. Opin. Chem. Biol.* **2,** 235–243
36. Kato, S., Shiratori, I., and Takamiya, A. (1962) *J. Biochem.* **51,** 32–40
37. Morand, L. Z., and Krogmann, D. W. (1993) *Biochim. Biophys. Acta* **1141,** 105–106
38. Braunschweiler, L., and Ernst, R. R. (1983) *J. Magn. Reson.* **53,** 521–528
39. Davis, D. G., and Bax, A. (1985) *J. Am. Chem. Soc.* **107,** 2820–2821
40. Bax, A., and Davis, D. G. (1985) *J. Magn. Reson.* **65,** 355–360
41. Griesinger, C., Otting, G., Wuthrich, K., and Ernst, R. R. (1988) *J. Am. Chem. Soc.* **110,** 7870–7872
42. Macura, S., and Ernst, R. R. (1980) *Mol. Phys.* **41,** 95
43. Wider, G., Macura, S., Kumar, A., Ernst, R. R., and Wuthrich, K. (1984) *J. Magn. Reson.* **56,** 207–234
44. Marion, D., and Wuthrich, K. (1983) *Biochem. Biophys. Res. Commun.* **113,** 967–974
45. Marion, D., Driscoll, P. C., Kay, L. E., Wingfield, P. T., Bax, A., Gronenborn, A. M., and Clore, G. M. (1989) *Biochemistry* **28,** 6150–6156
46. Sklenar, V., Piotto, M., Leppik, R., and Saudek, V. (1993) *J. Magn. Reson. Ser. A* **102,** 241–245
47. Bartels, C., Xia, T., Billeter, M., Guntert, P., and Wuthrich, K. (1995) *J. Biomol. NMR* **6,** 1–10
48. Guntert, P., Braun, W., and Wuthrich, K. (1991) *J. Mol. Biol.* **217,** 517–530
49. Guntert, P., Mumenthaler, C., and Wuthrich, K. (1997) *J. Mol. Biol.* **273,** 283–298
50. Jorgensen, W. L., Chandrasekhar, J., Madura, J. D., Impey, R. W., and Klein, M. L. (1983) *J. Chem. Phys.* **79,** 926–935
51. Case, D. A., Pearlman, D. A., Caldwell, J. W., Cheatham, T. E. III, Ross, W. S., Simmerling, C. L., Darden, T. A., Merz, K. M., Stanton, R. V., Cheng, A. L., Vincent, J. J., Crowley, M., Tsui, V., Radmer, R. J., Duan, Y., Pitera, J., Massova, I., Seibel, G. L., Singh, U. C., Weiner, P. K., and Kollman, P. A. (1999) AMBER 6, University of California, San Francisco
52. Bertini, I., Bryant, D. A., Ciurli, S., Dikiy, A., Fernandez, C., Luchinat, C., Safarov, N., Shumilin, S., Vila, A. J., and Zhao, J. (2001) *J. Biol. Chem.* **276,** 47217–47226
53. Alt, J., and Herrmann, R. G. (1984) *Curr. Genet.* **8,** 551–557
54. Schmitz-Linneweber, C., Maier, R. M., Alcaraz, J. P., Cottet, A., Herrmann, R. G., and Mache, R. (2001) *Plant Mol. Biol.* **45,** 307–315
55. Peitsch, M. C. (1996) *Biochem. Soc. Trans.* **24,** 274–279
56. Guex, N., and Peitsch, M. C. (1997) *Electrophoresis* **18,** 2714–2723
57. Altschul, S. F., Madden, T. L., Schaffer, A. A., Zhang, J., Zhang, Z., Miller, W., and Lipman, D. J. (1997) *Nucleic Acids Res.* **25,** 3389–3402
58. Huang, X., and Miller, W. (1991) *Adv. Appl. Mathematics* **12,** 337–357
59. van Gunsteren, W. F., Hünenberger, P. H., Mark, A. E., Smith, P. E., and Tironi, I. G. (1995) *Comput. Phys. Commun.* **91,** 305–319
60. Sainz, G., Carrell, C. J., Ponamarev, M. V., Soriano, G. M., Cramer, W. A., and Smith, J. L. (2000) *Biochemistry* **39,** 9164–9173
61. Banci, L., Bertini, I., Ciurli, S., Dikiy, A., Dittmer, J., Rosato, A., Sciara, G., and Thompsett, A. R. (2002) *Chembiochem* **3,** 299–310
62. Laskowski, R. A., MacArthur, M. W., Moss, D. S., and Thornton, J. M. (1993) *J. Appl. Crystallogr.* **26,** 283–291
63. Sippl, M. J. (1993) *Proteins Struct. Funct. Genet.* **17,** 355–362
64. Morris, G. M., Goodsell, D. S., Halliday, R. S., Huey, R., Hart, W. E., Belew, R. K., and Olson, A. J. (1998) *J. Comput. Chemistry* **19,** 1639–1662
65. Kurnikov, I. V. (2000) HARLEM 1.0, Department of Chemistry, University of Pittsburgh, Pittsburgh, PA
66. Donaire, A., Jimenez, H. R., Moratal, J. M., De la Rosa, M. A., Hervas, M., Navarro, J. A., Monleon, D., Tejero, R., and Celda, B. (1998) *Inorg. Chim. Acta* **275–276,** 73–89
67. Bertini, I., Ciurli, S., Dikiy, A., Fernandez, C., Luchinat, C., Safarov, N., Shumilin, S., and Vila, A. (2001) *J. Am. Chem. Soc.* **123,** 2405–2413
68. Xue, Y., Okvist, M., Hansson, O., and Young, S. (1998) *Protein Sci.* **7,** 2099–2105
69. Deleted in proof
70. Matias, P. M., Saraiva, L., Soares, C. M., Coelho, A. V., Le Gall, J., and Carrondo, M. A. (1999) *J. Biol. Inorg. Chem.* **4,** 478–494
71. Hervas, M., Navarro, J. A., Diaz, A., Bottin, H., and De La Rosa, M. A. (1995) *Biochemistry* **34,** 11321–11326
72. Mamedov, M. D., Mamedova, A. A., Chamorovsky, S. K., and Semenov, A. Y. (2001) *FEBS Lett.* **500,** 172–176A. Y.
73. Ubbink, M. (2004) *Photosynth. Res.* **81,** 277–287
74. Modi, S., He, S., Gray, J. C., and Bendall, D. S. (1991) *Biochim. Biophys. Acta* **1101,** 64–68
75. Joliot, P., and Joliot, A. (2002) *Proc. Natl. Acad. Sci. U. S. A.* **99,** 10209–10214
76. Mamedov, M. D., Vitukhnovskaia, L. A., Zaspa, A. A., and Semenov, A. Y. (2003) *Biofizika* **48,** 1044–1051A. Y.
77. Illerhaus, J., Altschmied, L., Reichert, J., Zak, E., Herrmann, R. G., and Haehnel, W. (2000) *J. Biol. Chem.* **275,** 17590–17595
78. Myshkin, E., Leontis, N. B., and Bullerjahn, G. S. (2002) *Biophys. J.* **82,** 3305–3313
79. Overfield, R. E., and Wraight, C. A. (1980) *Biochemistry* **19,** 3322–3327
80. Drachev, L. A., Mamedov, M. D., Mulkidjanian, A. Y., Semenov, A. Y., Shinkarev, V. P., and Verkhovsky, M. I. (1989) *FEBS Lett.* **245,** 43–46A. Y.
81. Drepper, F., Hippler, M., Nitschke, W., and Haehnel, W. (1996) *Biochemistry* **35,** 1282–1295

Structure of the Intermolecular Complex between Plastocyanin and Cytochrome *f* from Spinach

Francesco Musiani, Alexander Dikiy, Alexey Yu Semenov and Stefano Ciurli

J. Biol. Chem. 2005, 280:18833-18841.
doi: 10.1074/jbc.M412760200 originally published online February 3, 2005
